Stevenson, E. I., Aciego, S. M., Chutcharavan, P., Parkinson, I. J., Burton, K. W., Blakowski, M. A., & Arendt, C. A. (2016). Insights into combined radiogenic and stable strontium isotopes as tracers for weathering processes in subglacial environments. *Chemical Geology*, *429*, 33-43. https://doi.org/10.1016/j.chemgeo.2016.03.008

# Insights into combined radiogenic and stable strontium isotopes as tracers for weathering processes in subglacial environments

E. I. Stevenson* [1, 2], S.M. Aciego [1], P. Chutcharavan [1], I.J. Parkinson [3], K.W. Burton [2], M.A. Blakowski [1], C.A. Arendt [1].

*[1] Department of Earth and Environmental Sciences, University of Michigan, 2534 C.C. Little Building, 1100 North University Avenue. Ann Arbor, MI. 48109-1005*
*[2] Now located at Department of Earth Sciences, Durham University, Science Labs, Durham DH1 3LE*
*[3] School of Earth Sciences, University of Bristol, Wills Memorial Building, Queen's Road, Clifton BS8 1RJ*

*Corresponding author: emisstev@umich.edu, emily.i.stevenson@durham.ac.uk (+441913342346)

**Abstract**

This study reports stable and radiogenic strontium isotope behaviour in the dissolved load and suspended sediments from the subglacial outflow of the Lemon Creek glacier (Juneau Ice Field, Alaska) over a single melt season. *In situ* measurements (discharge, total alkalinity, pH and conductivity) are combined with elemental concentrations, X-Ray Diffraction (XRD) analysis and radiogenic strontium isotope measurements to interpret the variations observed in stable strontium isotopic ratios.

The stable Sr isotope composition ($^{88}Sr/^{86}Sr$ ratio expressed as $\delta^{88/86}Sr$, ‰) of the dissolved load averages 0.31 ± 0.05 ‰, and is heavier than both the suspended sediment 0.18 ± 0.03 ‰, as well as local bedrocks ~0.20 to 0.26 ‰. We attribute the enrichment of heavier isotopes in the dissolved load to the uptake of lighter Sr isotopes by secondary weathering minerals, driving the dissolved load to heavier values. X-Ray diffraction (XRD) analysis confirms the presence of clays in the suspended sediments and thermodynamic modelling suggests the presence of iron oxy-hydroxide phases. Although it is not possible to completely rule out the effect of dissolution of primary minerals in controlling Sr isotopic compositions of the dissolved load, our data indicate that the extent of secondary mineral formation likely plays a significant role. The preferential weathering of minerals such as biotite (consistent with the mineralogical assemblages found in the suspended sediments), as well as the potential presence of radiogenic calcites from metacarbonates (derived from the Yukon-Tanana terrain), may be driving the small seasonal shifts in $^{87}Sr/^{86}Sr$ of the dissolved load to more radiogenic compositions, from $^{87}Sr/^{86}Sr_{(DL)}$ = 0.71048 to 0.710647.

Using the combination of stable and radiogenic strontium isotopes to investigate weathering processes shows that radiogenic Sr isotopes provide information regarding weathering of primary phases. While the stable Sr isotope data appear to record information regarding the extent of secondary mineral formation, where secondary minerals incorporate the light isotopes, driving the dissolved load to heavy values.

## 1. Introduction

Glaciers are one of the most effective agents of erosion on Earth, generating vast quantities of fine particles with fresh reactive mineral surfaces that are susceptible to chemical weathering (Fairchild et al., 1994; Tranter et al., 1993). Sediment-water interactions are crucial to understanding glacial meltwater chemistry (Brown et al., 1994a; Fairchild et al., 1999; Tranter et al., 1993), as the rapid flow of water over these reactive surfaces maximizes both rates of chemical weathering and erosion. Glaciated outflows are dominated by high calcium, potassium and sulphate concentrations, (Anderson et al., 1997; Tranter, 2003), reflecting high physical and low chemical weathering rates occurring in the subglacial environment, and resulting in incongruent and non-stoichiometric chemical weathering processes (Anderson et al., 1997; Tranter, 2003).

Stable isotopes variations in group I and II metals have been successfully investigated as tracers of weathering processes in proglacial environments, for example lithium ($\delta^{7}$Li, e.g. Pogge von Strandmann et al. (2006) and Wimpenny et al. (2010)) magnesium ($\delta^{26}$Mg, e.g. Tipper et al. (2012) and Wimpenny et al. (2011), and calcium ($\delta^{44}$Ca, e.g. Hindshaw et al. (2008) and Hindshaw et al. (2011)). Stable strontium isotopes have also emerged as an additional proxy for tracing chemical weathering (Chao et al., 2015; de Souza et al., 2010; Pearce et al., 2015; Wei et al., 2013). The traditional radiogenic strontium ($^{87}Sr/^{86}Sr$) system has been applied to glacial outflow waters as a proxy for mineral weathering reactions and processes (e.g. Anderson et al. (2000), Arn et al. (2003), Hagedorn and Hasholt (2004) and Sharp et al. (2002)), and also to further understand connections between Sr isotope ratios in glacial runoff and the variation in the Sr isotope composition preserved in marine biogenic carbonates, which are widely regarded as the most well understood proxy of continental Sr fluxes to the ocean (Hagedorn and Hasholt, 2004). Chemical weathering associated with glaciers has attracted much attention due to the possible link between increased chemical weathering during glacial retreat and control of the marine radiogenic strontium ($^{87}Sr/^{86}Sr$) ratios (e.g. Armstrong (1971), Capo and Depaolo (1990), Mokadem et al. (2015) and Vance et al., 2009) and the potential for negative feedbacks to global climate through the carbon cycle (Anderson et al., 2000; Blum and Erel, 1995).

Analytical advances have increased the potential utility of stable strontium isotopes because they permit the measurement of small, yet resolvable mass dependent fractionations in the $^{88}Sr/^{86}Sr$ ratios in natural materials (e.g. Fietzke and Eisenhauer (2006), Krabbenhöft et al. (2009), Ohno et al. (2008) and Rüggeberg et al. (2008). Whilst this proxy is still being developed, data for natural samples and rock standards indicate that $\delta^{88/86}$Sr ($\delta^{88/86}Sr = ((^{88}Sr/^{86}Sr)_{SAMPLE}/(^{88}Sr/^{86}Sr)_{NBS987})-1)\times1000$) preserves a broad range of values ranging between +0.1 to -0.3 ‰ for terrestrial carbonate rocks (Halicz et al., 2008; Ohno et al., 2008), +0.05 ‰ to +0.35 ‰ for biogenic marine carbonates (e.g. Fietzke and Eisenhauer (2006), Halicz et al. (2008), Rüggeberg et al. (2008) and Stevenson et al. (2014)) and +0.2 to +0.3 ‰ for terrestrial silicate rocks (Charlier et al., 2012; Ma et al., 2013; Moynier et al., 2010). More recently barites have been shown possess values between +0.07 to +0.11 ‰ (Widanagamage et al., 2014). Measurable mass dependent fractionations of $\delta^{88/86}$Sr can occur during terrestrial exogenic cycling with lighter strontium isotopes preferentially incorporated into substrates including, but not limited to: biogenic and inorganic calcium carbonates (e.g. Böhm et al. (2006), Fietzke and Eisenhauer (2006), Rüggeberg et al. (2008) and

Stevenson et al. (2014)); other secondary minerals (Halicz et al., 2008) and terrestrial plants (de Souza et al., 2010). de Souza et al. (2010) measured $\delta^{88/86}$Sr in a glaciated granitic watershed, with results indicating no resolvable fractionation between bulk soils and bedrock. However the authors argued this was because of the chemical heterogeneity of the forefield, and that due to incipient silicate weathering the soils have thus far witnessed nominal net loss of Sr. In addition to potential source variation in stable strontium isotopes from the dissolution of bedrock in the glacial environment, natural and experimental studies have shown that during the crystallization of calcium carbonate Sr isotopes undergo mass dependent fractionation whereby the lighter strontium isotopes are preferentially incorporated into the carbonate phase and therefore have lighter $\delta^{88/86}$Sr values than the fluid phase (e.g. Bohm et al. (2012) and Fietzke and Eisenhauer (2006). Therefore, the stable strontium isotope composition of complementary bedrock, suspended sediments and the dissolved load accompanying glacial weathering may vary significantly due to (i) the intensity of physical and chemical weathering of source primary minerals, (ii) a change in rate or extent of secondary mineral formation, (iii) a change in the balance of these dissolution and precipitation reactions, and (iv) adsorption/desorption processes associated with clays or other secondary minerals.

Rates of subglacial chemical weathering vary with the timing of the melt season; at the onset of the melt season, surface derived meltwater begins to reach the ice-rock interface, which can result in an increase in water stored at the glacier bed, and promote longer water-rock contact times leading to an increase in chemical weathering (Benn and Evans, 2010). During peak melting, a well-developed hydrological network system will increase the meltwater flow-through speed, decrease the residence time within the glacier and lower the water-rock interaction times (e.g. Fountain and Walder (1998) and Tranter (2003)). Therefore we may see variations in the radiogenic and stable Sr isotope ratios associated with seasonal changes in the subglacial network caused by: (i) faster mineral dissolution kinetics due to the lengthening of subglacial channels over fresh unweathered bedrock; (ii) variations in bedrock composition and weathering rates of the minerals present, (iii) differing water-rock interaction times, and/or (iv) sediment residence times in discrete pockets of subglacial water.

Radiogenic strontium isotopes tend to behave conservatively during the short time period of a glacial melt season, with variation potentially resulting from reactive mineral dissolution, which reflects the subglacial lithology and weathering intensity. This study documents a seasonal record of both the radiogenic and stable Sr isotope compositions of the dissolved load (DL) and suspended sediments (SS) from a glaciated environment in southeast Alaska. Using a high precision double spike isotope technique (e.g. Krabbenhöft et al. (2009) and Stevenson et al. (2014)) we provide insights into the weathering of primary minerals such as biotite, using radiogenic Sr isotopes, and the formation of secondary weathering minerals, such as clays, using stable Sr isotopes.

## 2. Sample site and regional geology

The Lemon Creek glacier (LCG) is a small valley glacier forming the southernmost extension of the Juneau Icefield, ~ 6.5 km northeast of Juneau, Alsaka (Figure 1(a)). The Juneau Icefield is

situated in the Tongass National Forest, part of the Coast Mountain Range of southeast Alaska, extending over an area of ~4,000 $km^2$. The LCG is small, less than 11.7 $km^2$ in size, and thus exhibits simple alpine glacier dynamics (Criscitiello et al., 2010). The LCG is unbranched and is orientated generally in N-S direction except near the toe where it curves west, see Figure 1 (b). Flow begins on the Northwest slope of Observation Peak (1512 m) and travels via an icefall between elevations of approximately 650 and 850 m (Heusser and Marcus, 1960). The LCG has undergone significant negative mass balance with a terminal retreat of over 700 m and a net surface height decrease of 24.7 m during the period 1953–1998 (Miller and Pelto, 1999). The LCG is situated within a maritime climate, and mass balance is strongly influenced by climatic parameters (temperature and precipitation), high winter snowfall, as well as the Pacific Decadal Oscillation (PDO), more so at the glacier terminus than in the accumulation zone (Criscitiello et al., 2010). The LCG covers approximately one third of the 32 $km^2$ Lemon Creek watershed, therefore seasonal fluctuations in discharge from this glacier can significantly impact the downstream Lemon Creek river which drains into Juneau.

Geologically, the LCG sits on the mid-Cretaceous central pluton-gneiss belt (Figure 1 (b)), with the immediate area comprised of young tonalite sills (50-70 Ma) to the west, high grade pre-Tertiary metamorphosed sedimentary and volcanic rocks surrounding the sample site, and late-Permian metamorphosed sedimentary rocks (Greenschist facies) are found to the east (Kistler et al., 1993). The geological units underlying the LCG are predominantly biotite schist, biotite gneiss, marble and calc-silicate granofels, hornblende gneiss and granotoid rocks (mainly tonalite/migmatite and biotite/hornblende tonalite) with a general age range of 62-69 Ma and an overall younging of bedrock in a northeasterly direction (Brew and Ford, 1985; Gehrels et al., 1984).

An additional input into the LCG system is Lake Linda, a supraglacial lake at the head of the LCG. Lake Linda is located on the Juneau Icefield (N 58°21.000', W 134°21.960') and drains annually through a composite englacial cave ~ 450 m long and out through the LCG terminus each summer melt season. During 2012 a reconnaissance flight revealed that on calendar day (CD) 213, Lake Linda had not drained, however a field excursion on CD 230 to sample Lake Linda revealed the lake had by this time drained.

## 3. Methods

### *3.1 Sample collection*

Prior to sampling, all sample containers and tubing were pre-cleaned (See Supplementary Information). Samples for Sr analysis were collected directly from the main subglacial outflow channel at the terminus of the Lemon Creek Glacier (Figure 1 (c) site A: N 58°24.455', W 134°22.296') on a daily basis from CD 223-252 in 2012 between 9 and 10 am. For subglacial water and suspended sediment (SS) collection one litre (L) of Super-Q > 18.2 MΩ·cm deionized (SQDI) water was filtered through the system prior to filtration of samples using a Masterflex modular peristaltic pump and a polycarbonate filtration unit (Geotech Environmental Equipment Inc.). Subglacial water was then pumped and filtered through polytetrafluoroethylene (PTFE)

filter (0.2 μm) membranes to remove the SS, and the resultant filtered water was then collected into the pre-cleaned 1L Nalgene bottles. Samples were acidified with Optima hydrochloric acid to a pH of < 2. Filter membranes containing the SS were archived into acid-cleaned centrifuge tubes.

Daily electrical conductivity, temperature, pH, and alkalinity measurements were also taken at the glacier terminus (Figure 1 (c) site A: N 58°24.455', W 134°22.296'), taken using a YSI Handheld Multiparameter Instrument (Pro Plus Multiparameter). Full methods are reported in Supplementary Information. Daily discharge measurements were made at the end of the glacial outflow where it fed Lake Thomas (Figure 1 (c) site B: N 58°24.410' W 134°22.266'). These were made manually using an Acoustic Doppler Velocimeter Flow-tracker (see Supplementary Information).

Four rock samples, considered representative of the local bedrock, were collected from the periphery of the site at the Lemon Creek glacier terminus. These comprised of a quartzite, gneiss, plutonic igneous granodiorite and a metamorphosed, crystalline carbonate.

*3.2 Sample preparation*

The water samples were evaporated to dryness on a hotplate in sufficient quantity to provide 2 μg Sr for isotope analyses for each sample. Suspended sediment was carefully removed from each filter with Super-Q > 18.2 MΩ·cm Deionized (SQDI) water and left on a hotplate until dry. Ten milligrams of dry sediment was weighed and digested for 7 days in 2 mL of concentrated nitric acid with 0.5 mL hydrofluoric acid. Samples were dried down and further digested in ultra-pure aqua regia for 24 hours to oxidize any residual organic material. The four rock samples, a tonalitic gneiss, metamorphosed and crystalline carbonate, quartzite, and a plutonic igneous granodiorite, were crushed, powdered and homogenised using a jaw crusher and a ceramic shatterbox. Ten to twenty milligrams of the resulting powder was weighed and dissolved using a Parr bomb digestion vessel**.** The sample was weighed into 3 mL Savillex beakers and 2 mL of concentrated hydrofluoric acid was added. The beakers were placed in a 125 mL PTFE flask and 7 mL of concentrated hydrofluoric acid with trace nitric acid was added. The vessel was then sealed and placed in the Parr bomb, and left in a 220°C oven for at least 48 hours followed by 12-16 hours in 12 M hydrochloric acid at 180°C for full dissolution. Blanks for both water and sediment processing were monitored using a known quantity of a laboratory $^{84}Sr$ spike. In addition a two rock standards, BCR-2, and SRM987 were used to quality check column chemistry and TIMS analysis, see section 3.4. Suspended sediment concentrations (mg $L^{-1}$) were calculated by carefully removing the suspended sediment from filter membranes, which had one litre of glacial outflow, pumped across them whilst in the field. After heating to dryness on a hotplate the suspended sediment was weighed and reported as mg $L^{-1}$.

*3.3 Cation analysis*

Cation concentrations (Ca, Na, Mg, K, Sr, Rb, Ba, Al and Fe) were determined by analyzing 3 mL of each water sample on the Thermo Scientific ELEMENT2 ICP-MS operating in pulse

counting mode, at the University of Michigan KECK Lab. An acid blank and a standard of known concentration were run as unknowns with every five samples; standards reproduced within error of the calibration curve and the acid blank was below detection limits. Each sample was measured in triplicate and internal analytical errors are <1%; external accuracy and reproducibility is provided by the periodic measurement of international reference standard NIST1640a, (see Aciego et al. (2015)). A limited data set of major elemental concentrations can also be found in Sheik et al. (2015).

*3.4 Strontium isotope analysis*

For stable and radiogenic strontium analysis of both water and sediment, 2 μg Sr was processed.. Each 2 μg Sr sample was split prior to column chemistry and one portion was spiked for stable Sr isotope analysis with a $^{84}Sr$-$^{87}Sr$ double spike. The sample was capped and left to equilibrate on a hot plate for 24 hours then dried down and redissolved in 500 μL 3 M $HNO_3$. Both spiked and un-spiked samples were loaded in 500 μL 3 M $HNO_3$ onto separate Sr columns containing 150 μL Eichrom Strontium specific resin bed in 500 μL 3 M $HNO_3$. The column was washed and eluted in several stages with $HNO_3$ following the procedure outlined by (Aciego et al., 2009). The total procedural Sr blank was less than ~60 pg, constituting < 0.1% of the total Sr analysed for a typical Sr analysis (sediment or water), quantified using an $^{84}Sr$ spike. Strontium samples were loaded onto outgassed 99.98% Re filaments in 1.0 μL concentrated $HNO_3$ along with 0.8 μL $TaF_5$ activator to enhance the ionization efficiency of Sr (Charlier et al., 2006). Strontium isotope measurements were carried out on a Thermo-Finnigan Triton Plus Thermal Ionisation Mass Spectrometer (TIMS) using the method outlined in Stevenson et al. (2014). For natural runs (un-spiked samples) any fractionation caused by the machine was corrected for using $^{86}Sr/^{88}Sr$ = 0.1194. External precision on the standard runs (NBS987) for $^{87}Sr/^{86}Sr$ was 0.710264 ± 0.000016 (2 s.d. n=50). A basalt rock (BCR-2) and a seawater standard (IAPSO; batch P141) were used to assess the precision of the column chemistry and analytical procedure. To calculate the stable Sr isotope composition, both spiked and un-spiked raw isotope data for each sample are deconvolved using the exponential fractionation law and a Newton-Raphson iterative technique (Albarède and Beard, 2004). The measured values of IAPSO and BCR-2 for $^{87}Sr/^{86}Sr$ were within error of literature values 0.70919 ± 3 (2 s.d. in the last decimal place, n=8) and 0.70504±5 (2 s.d. in the last decimal place, n=3), respectively (e.g. Krabbenhöft et al. (2009), Ma et al. (2013) and Moynier et al. (2010)). The IAPSO seawater standard yields a $\delta^{88/86}Sr$ value of +0.38 ± 0.03 ‰ (n=8) and is within error of other modern day seawater measurements (e.g. de Souza et al. (2010), Fietzke and Eisenhauer (2006) and Krabbenhöft et al. (2010)). BCR-2 gave a $\delta^{88/86}Sr$ value of +0.28 ± 0.05 ‰ (n=3), indistinguishable from values obtained elsewhere (e.g Ma et al. (2013) and Moynier et al. (2010).

*3.5 X-Ray Diffraction analysis*

The mineralogy of the suspended sediment was determined by taking 100 to 500 mg splits of suspended sediment collected on the filter that were then powdered using a mortar and pestle and transferred to glass sample holders. Approximately 20 samples were measured using a Rigaku Ultima IV X-ray diffractometer. Raw data was then analyzed, and processed using Rigaku

263 software (PDXL). Minerals were identified using peak standards from the ICDD PDF-2 2008
264 database to determine the mineralogy of each sample.
265
266 **4. Results**
267
268 *4.1 Physiochemical properties*
269
270 Details on the physiochemical properties of glacial outflow can be found in Supplementary
271 Information, in summary: Conductivity, pH and alkalinity all stay fairly constant (10.2 μS, 7.15
272 and 6.6 ppm $CaCO_3$ respectively) until CD 235 where over a period of 4-6 days these parameters
273 begin to increase (8.1-17.4 μS, 6.7-8.2 and 5.0-12.2 ppm $CaCO_3$ respectively) however these do
274 not coincide with spikes in air temperature, water temperature, rainfall or discharge (Figure 2 (a),
275 and Supplementary Information). Discharge from the LCG remains fairly constant throughout the
276 season (approximately 2 $m^3 s^{-1}$, Figure 2 (b) and Supplementary Information). Sediment load
277 decreases between CD 227-235 from 136 mg $L^{-1}$ to 11 mg $L^{-1}$ (Figure 2 (b)), however the
278 seasonal average is approximately 100 mg $L^{-1}$ excluding an anomalously high peak of 629 mg $L^{-1}$
279 on CD 248. Strontium concentrations of the DL are shown in Figure 2 (a) along side conductivity
280 measurements for comparison, and show similar seasonal trends. Cations increase at CD 235
281 (Table 1), and then plateau from approximately CD 240, coinciding with increases in
282 conductivity, pH and alkalinity. Calcium and Mg are positively correlated ($R^2 = 0.99$). The Ca/Na
283 and Mg/Na ratios average 15.4 and 1.35 mol/mol, and both trend to higher values during the
284 period of CD 225–238 and are positively correlated with $R^2 = 0.93$.
285
286 *4.2 Strontium isotopes*
287
288 *4.2.1 Radiogenic strontium isotopes*
289
290 We present the conventional $^{87}Sr/^{86}Sr$ ratios normalized to $^{86}Sr/^{88}Sr = 0.1194$ and not the $^{86}Sr/^{88}Sr$
291 corrected $^{87}Sr/^{86}Sr^*$ notation (Krabbenhöft et al., 2009). The radiogenic Sr isotopes in the DL and
292 SS trend to more radiogenic values as the season progresses (Figure 2 (d)). The DL is consistently
293 more radiogenic than its SS counterpart: $^{87}Sr/^{86}Sr_{(DL)} = 0.710483 \pm 5$ to $0.710647 \pm 5$; $^{87}Sr/^{86}Sr_{(SS)}$
294 $= 0.70903 \pm 6$ to $0.70969 \pm 2$ (errors are 2 standard errors in the last decimal place for all reported
295 $^{87}Sr/^{86}Sr$ measurements). We observe similar seasonal trends in both the DL and SS, however
296 $^{87}Sr/^{86}Sr_{(SS)}$ excursions are larger than $^{87}Sr/^{86}Sr_{(DL)}$. Repeat measurements of the DL samples were
297 predominantly within error of each other; see Table 1. However, reproducibility for some of the
298 SS was not as good (up to 3 ‰ variation), compared to the DL (<0.02 ‰ variation) likely
299 because samples were not completely homogenized when a sub-sample was removed.
300
301 Four representative bedrock samples yield the following values; quartzite ($0.72960 \pm 1$), gneiss
302 ($0.70761 \pm 4$), a plutonic igneous granodiorite ($0.70710 \pm 4$), and a metamorphosed, crystalline
303 carbonate ($0.70800 \pm 2$), similar to the $^{87}Sr/^{86}Sr$ ratios measured in the Juneau Gold Belt 0.7082
304 (carbonate) to 0.8091 (phlogopite), by Kistler et al. (1993).
305
306 *4.2.2 Stable strontium isotopes*

The stable Sr isotopes of both the DL and SS reveal little seasonal related variation with average $\delta^{88/86}Sr$ values of $\delta^{88/86}Sr_{(DL)} = 0.31 \pm 0.05$ (errors reported as two standard errors, see Table 1) and $\delta^{88/86}Sr_{(ss)} = 0.18 \pm 0.03$ respectively (Table 1 and Figure 2 (c)). The suspended load is consistently lighter than the corresponding DL sample by 0.1 to 0.2 ‰ throughout the season. The stable Sr values for the DL range start at $\delta^{88/86}Sr_{(DL)} = 0.31 \pm 0.01$ ‰ and fluctuate as the season progresses with the heaviest values found at CD 247 ($\delta^{88/86}Sr_{(DL)} = 0.40 \pm 0.02$ ‰). The sediment values range from $\delta^{88/86}Sr_{(SS)} = 0.12 \pm 0.02$ ‰ to $0.25 \pm 0.02$ ‰ but additionally show little trend as the season progresses. $\delta^{88/86}Sr$ for both the DL and SS decreases between CD 229 through to CD 241 (Figure 2 (c)). The three rock samples were analysed for stable Sr and the results are: the tonalitic gneiss sample $0.20 \pm 0.01$ ‰, a plutonic igneous granodiorite, $0.26 \pm 0.01$ ‰ and a metamorphosed, crystalline carbonate $0.24 \pm 0.02$ ‰ (Figure 4). No measurement was made of the quartzite due to the minimal sample size and loss of the sample during analysis.

*4.3 X-Ray Diffraction (XRD)*

The XRD analysis of Lemon Creek Glacier SS demonstrates that the mineral phases present in the sediment remained fundamentally constant throughout the study period (see Supplementary Information). All samples contain quartz, plagioclase, biotite, hornblende, and chlorite. Clinopyroxene (cpx) and various clay minerals (e.g. vermiculite, montmorillonite) were detected in most samples, and calcite was present in four of the thirteen samples. Overall, the bulk SS composition appears to be sourced from two distinct lithologies: firstly plagioclase, hornblende, clinopyroxene and biotite which derive from the weathering of the foliated hornblende-biotite tonalite sills (Ingram and Hutton, 1994). Secondly, the presence of quartz, additional clay minerals and calcite suggest that the metamorphosed sedimentary and volcanic rocks surrounding the study site, from the Yukon-Tanana terrain are also a source for the sediment. It is difficult to quantify mineral abundances within each bulk sediment, particularly for samples with such a complex mineralogy, therefore we are limited in our conclusions as no further inferences can be made without a quantitative estimate of mineral abundances.

## 5. Discussion

*5.1 Physiochemical and hydrochemical properties*

Daily discharge velocities over the field season remained similar to the mean channel discharge of approximately 2 $m^3 s^{-1}$, suggesting a fairly stable subglacial network (Figure 2 (a)). However, the sediment load shows significant variations, which has implications for the location and magnitude of solute acquisition and secondary weathering processes. The initial decline to 11 mg $L^{-1}$ at CD 235 followed by a recovery to an average of 100 mg $L^{-1}$ from CD 236 onward correlates with spikes in the *in situ* data, elemental concentrations and radiogenic ratios (Supplementary information, Table 1 and Figure 2 (a-b)). Taken together this suggests that whilst the hydrological flux is fairly constant (inferred from discharge measurements), the sediment source or sediment residence time is changing over the melt season.

Calcium is the major cation in the LCG subglacial outflow and is positively correlated with alkalinity ($R^2 = 0.8$) suggesting that calcite dissolution is a source of Ca, despite the silicate-based bedrock. Rubidium (Rb) tends to partition into K-rich in minerals such as K-feldspar and biotite, whilst Sr tends to be enriched in Ca-bearing minerals. In rivers draining Alpine glaciers, it has been inferred that high K/Na ratios (> 1.0) in the melt runoff result from the leaching of interlayer cations from biotite (Anderson et al., 2000). The K/Na ratios remain above one, suggesting additional input from biotite into the bulk subglacial outflow. At the beginning of the season the Rb/Sr stays constant at approximately 0.09, until CD 237 when the Rb/Sr continually decreases to approximately 0.065, indicating a decrease in the silicate weathering component, or an increase in the weathering of mineral with a low Rb content.

Towards the end of the sample season, the meltwater generated may not be sufficient to cause flow velocities similar to those at the peak of the melt season resulting in heightened water-rock interaction times, increasing solute acquisition from sediments and increase elemental concentrations (Nienow et al., 1996). We see a spike in elemental concentrations concurrent with increases in pH, alkalinity and conductivity post CD 235, however there are no simultaneous increases, or decreases in discharge. This may be due to (i) decreased meltwater through the subglacial system post peak melt, (ii) mixing of channelized meltwater with distributed subglacial water from a differently routed water mass (iii) expansion of the subglacial system over fresh physically weathered bedrock.

### *5.2 Strontium isotopes*

#### *5.2.1 Radiogenic Sr isotopes*

The radiogenic strontium isotope composition of the DL is more radiogenic than that of the SS, indicative of incongruent weathering processes. Both the DL and the SS show seasonal progression to more radiogenic values, however the transition is much more pronounced for the SS, in particular from CD 235 onward. For riverine systems, seasonality has been shown to have a large impact on dissolved radiogenic Sr ratios (e.g. Douglas et al. (2013) and Voss et al. (2014)). For example, during spring and summer snowmelt the overall composition of material exported to the ocean by the Fraser River is weighted disproportionately to material derived from the most upstream portions of the drainage basin (Voss et al., 2014). At the beginning of the melt season, a more distributed, less efficient network can have a sediment transport capacity far less than the available supply and therefore is assumed to produce low sediment fluxes (Hodson and Ferguson, 1999; Swift et al., 2005). Conversely, as the drainage system becomes better developed throughout the season, it will have higher transport capacities and sediment fluxes (Swift et al., 2005). This may continue until the subglacial sediment supply is diminished and sediment fluxes decline or the drainage channels start to collapse at the end of the melt season (Hodson and Ferguson, 1999). Therefore what we observe as a seasonal transition in the radiogenic Sr values, maybe related to a shift in the size and length of the subglacial network.

Field studies have shown that post-mixing reactions with suspended sediment occur when rapidly flowing waters dilute delayed flow in arterial conduits at the glacier bed (Brown et al., 1994b), as

the melt season progresses the conduit system becomes more extensive and the suspended sediment increases in the melt water. The excursions of the $^{87}Sr/^{86}Sr$ of the suspended sediment, from CD 236, combined with the in situ field data and elemental concentrations suggests that the predominant hydrological source likely changed. However these assumptions are impacted by the subglacial drainage morphology which is currently unconstrained, and therefore it is difficult to determine whether the assumed changes in the radiogenic isotope signatures of the suspended sediment are due to changes in transport efficiency, sediment supply changes or variations in mineralogy. The XRD data suggests that bulk mineralogy stays essentially the same; therefore we may infer that the source of the sediment has not changed but perhaps its residence within the subglacial system has.

With the exception of the quartzite sample, both the DL and SS are more radiogenic than the bedrocks measured consistent with the preferential weathering of radiogenic mineral phases such as biotite or amphibole. Due to the radiogenic nature of the quartzite, it may possibly have a lower Sr content, but may be more resistant weathering and thus may minimally impart solute to the dissolved load compared to more soluble minerals such as carbonates. The presence of biotite in the bedrock geology underlying the glacier (see Section 2) is confirmed by XRD measurements of the mineral assemblages of the SS. Radiogenic Sr ratios in the DL, if derived from biotite, should be associated with high Rb/Sr ratios, however we observe a negative correlation of $^{87}Sr/^{86}Sr$ with Rb/Sr in the dissolved load (Figure 3 (a)).

Carbonate minerals, such as calcite tend to have a high Ca/Mg ratio; as the season progresses we see an increase to higher Ca/Mg ratios indicating an increase in the weathering of calcite into the DL (Figure 3 (b)). Sediment production and transport are influenced by the nature of the hydrological system (Hooke, 1989). Over a given residence time in the subglacial environment the $^{87}Sr/^{86}Sr$ composition of the DL is representative of the entire flow path, integrating the initial $^{87}Sr/^{86}Sr$ ratio of the under-saturated meltwater and its flow throughout the subglacial system. However, the $^{87}Sr/^{86}Sr$ composition of SS may be modified by incongruent dissolution during subglacial transport as well as the sediment carrying capacity of the hydrologic network, which may also vary seasonally. Where the flow of the subglacial water slows, SS can be deposited and larger size fractions settle out. In areas where flow increases, new material can be added to suspension by erosion. Seasonal variations in subglacial drainage morphology complicates our ability to determine whether changes in the radiogenic isotope signatures of the SS are due to a change in mineralogy, sub-glacial transport efficiency, or sediment supply.

X-Ray diffraction analyses indicate that biotite is present, and that the bulk mineralogy of the SS essentially remains constant. Taken together our data suggests the presence of biotite, the weathering of which can provide a source of radiogenic Sr to the dissolved load. Whether, Rb/Sr ratios change as a result of weathering depends on the differential dissolution of the minerals in the particular bedrock studied (Dasch, 1969). There is an unidentified source of carbonate to the outflow (inferred from the seasonal change in Rb/Sr and Ca/Mg ratios (Figure 3 (a-b)), despite the increases to more radiogenic ratios. Therefore, in order to explain this simultaneous shift to lower Rb/Sr ratios, but more radiogenic Sr, an alternate hypothesis is needed. Once possibility is the occurrence of metamorphosed limestone, with a radiogenic Sr isotope composition in the

Yukon-Tanana terrain, similar to that found in the catchments of the Yukon and Alaskan rivers, ranging from $^{87}Sr/^{86}Sr$ 0.70422 to 0.74041 (Brennan et al., 2014) and 0.70934 to 0.7230 (Millot et al., 2003),which additionally tend to be Mg and Ca rich, and would drive the dissolved load to more radiogenic values. High physical weathering rates supply freshly comminuted mineral surfaces. Under these conditions, chemical weathering is limited to the most reactive minerals, such as carbonates and not necessarily the most abundant, which may be providing the majority of solute (Anderson et al., 2000; Anderson et al., 1997; White et al., 2005). In these circumstances we might expect the dissolved load to become more radiogenic with an enhancement of carbonate weathering from increasingly exposed Yukon-Tanana terrain (see Figure 1 (b)) in the subglacial environment during the melt season.

*5.2.2 Stable strontium isotopes*

The radiogenic strontium isotopes of the DL and SS are unaffected by secondary weathering processes, therefore seasonal variation is ascribed to variations in either the source of material being weathered or weathering congruence. Variation in the stable strontium isotopes can be associated with either mass dependent fractionation during weathering or mixing of sources with distinctive stable strontium isotope ratios. The work presented here is the first application of stable strontium isotopes to examine a seasonal progression of weathering in a subglacial system.

*5.2.2.1 Seasonal progression*

Over the course of the melt season the stable Sr isotope composition of the DL ranges from 0.26 ± 0.02 to 0.40 ± 0.02 ‰ with most of the data centered around the flux-weighted global river average of 0.315 ± 0.008 ‰ (Krabbenhöft et al., 2010), see Figures 2 and 4. The range of $\delta^{88/86}Sr$ in the DL additionally lies within the range of three major drainage basins draining the southeast Alaskan region, the Frazer, Nass and Stikine with $\delta^{88/86}Sr$ of 0.256 ± 0.007, 0.296 ± 0.007 and 0.296 ± 0.007 ‰ respectively (Pearce et al., 2015). There appears to be a negative trend to lighter values between CD 227 to 242, and then an excursion to heavier values, reaching a maximum at CD 245. The SS also appears to trend towards lighter compositions as the season progresses, but the data is more scattered. Where we observe increases in the conductivity and radiogenic ratios (CD 235) the $\delta^{88/86}Sr$ of both the DL and SS decreases, however this appears to become decoupled beyond CD 242.

The composition and mineralogy of the bedrock underneath the glacier should determine the initial isotope composition of the DL during mineral dissolution. As discussed for the radiogenic Sr compositions, subglacial weathering often results in the preferential weathering and dissolution of phases such as biotite, calcite and sulphide (Anderson et al., 1997; Tranter, 2003), therefore these phases can potentially dominate the meltwater chemistry. Data from a seasonal progression presented by Wei et al. (2013) suggests the weathering of carbonates drives river waters to lighter $\delta^{88/86}Sr$ compositions and intensive silicate weathering to heavier compositions, varying from 0.147 to 0.661 ‰. Based on these inferences, we assume carbonate materials have a high Ca/Mg value and lower $\delta^{88/86}Sr$, and silicates have low Ca/Mg and heavier $\delta^{88/86}Sr$. As the season progresses Ca/Mg increases with indicating an increase in a carbonate component to the DL,

however whilst there is variability in the $\delta^{88/86}$Sr composition (Figure 3 (c)), there is no significant relationship between them. Therefore, this trend could be indicative of both changes in source and weathering intensity (similar to the radiogenic Sr ratio). The greatest input of un-weathered minerals into the glacial system probably occurs during the summer melt season when material is drained from beneath the glacier (Tipper et al., 2012). Water fluxes through the glacial hydrological network tend to be at their highest during peak melt and kinetic isotope effects are enhanced as there is less time to reach equilibrium (Tipper et al., 2012). Development in the size and efficiency of the subglacial hydrological network over the melt season may cause a change in the composition of the meltwater due to a shift in the source of bedrock or a shift in weathering congruence, or a mix of both these processes. The field campaign during the summer of 2012 fell over a ninety-day period (CD 122–213) that saw the lowest average daily high temperatures in Juneau in 69 years (NOAA, 2014). One consequence of this colder melt season may be that the SS and DL do not reflect the usually signal seen over a full seasonal. For example, we see no peaks in discharge representing a significant period of 'peak melt'. In this case, the results presented here may be more representative of strontium isotope compositions during the initial stages of mineral weathering in the subglacial environment, rather than a typical full melt season.

*5.2.2.2 Causes of stable strontium isotope fractionation*

Mass dependent fractionation of non-traditional stable isotope systems (e.g. $\delta^{26}$Mg, $\delta^{44}$Ca and $\delta^{7}$Li) during chemical weathering can occur due to dissolution, precipitation, sorption of metals onto the surfaces of minerals, and the effect of the coordination environment. Recent studies have suggested that for the $\delta^{88/86}$Sr system fractionation between the dissolved load, sediments and host rocks occurs via the preferential leaching of heavy Sr into the hydrosphere leaving light Sr in residual soils (Chao et al., 2015; Pearce et al., 2015). Similar to the $\delta^{88/86}$Sr study of Chao et al. (2015), we find the dissolved load is heavier than local bedrocks and the suspended sediments. The stable Sr composition of the SS is lighter than the DL: they are not correlated but show a similar total $\delta^{88/86}$Sr range of 0.14 and 0.12 ‰ respectively. The stable Sr isotope measurements of the SS here overlap with the average silicate earth value of $\delta^{88/86}$Sr 0.27 ± 0.05 ‰ (Moynier et al., 2010), Figure 4, and are lighter than that of the local bedrock measured here. The tonolitic gneiss and the granodiorite are within error of previously measured gneissic and granitic samples from the Damma Glacier, Switzerland (de Souza et al., 2010). These rock values, 0.24, 0.31 and 0.18 ‰, lie between the average DL and SS. However we were unable to make a stable strontium isotope measurement of the quartzite. Stable strontium analysis of a suite of rock standards and terrestrial materials from Charlier et al. (2012) showed terrestrial rocks have a fairly uniform composition of +0.30 ± 0.07 ‰ (2 s.d.), and highly evolved melts from andesites to high-silica rhyolites have lighter $\delta^{88/86}$Sr compositions, ranging from 0.19 to -0.19 ‰ and represent the only terrestrial silicates to have light $\delta^{88/86}$Sr values. In particular, the K-feldspar standard (NBS 607) analyzed by Charlier et al. (2012) has a negative $\delta^{88/86}$Sr value of -0.07 ± 0.06 ‰ (2 s.d.). In comparison, the $\delta^{88/86}$Sr composition of the SS tend to lighter values than the rocks analyzed from the Lemon Creek area, and are also lighter then range of the average silicate Earth (Moynier et al., 2010). Because we are unable to sample the inaccessible rocks beneath the glacier it is impossible to say whether those samples would support or negate our current explanation.

However, it may be possible that there is a missing rock assemblage that has a significantly lighter composition, potentially a calcite or celestine, which is driving the SS to lighter values.

For stable strontium isotopes the direction of fractionation seen here, where the SS is lighter than bedrock, appears most similar to the $\delta^7$Li system. Although studies of adsorption related to stable strontium isotope fractionation are limited, laboratory experiments indicate that the lighter Sr isotopes are preferentially adsorbed onto humid acid coated magnetic nano iron oxide particulates, leaving heavier $\delta^{88/86}$Sr isotopes in the residual solution (Liu et al., 2012). For $\delta^7$Li compositions the DL is not always related directed to basin lithology, but rather the intensity and regime of silicate mineral weathering (e.g. Millot et al. (2010), Pogge von Strandmann et al. (2006) and Vigier et al. (2008)). Wimpenny et al. (2010) hypothesized that $\delta^7$Li fractionation between SS and DL arises via the formation of Fe-(oxy)hydroxides as a product of sulphide oxidation. The (oxy)hydroxides preferentially uptake $^6$Li onto the mineral surface driving the DL to heavier isotopic compositions. If the lighter isotopes of strontium were adsorbed onto (oxy)hydroxide phases, this would drive the DL to heavier compositions. Subsequently, if (oxy)hydroxide phases become incorporated into suspended and particulate materials bulk $\delta^{88/86}$Sr isotope compositions of the measured SS would become isotopically lighter, potentially lighter than that of the bedrock from which it was derived (illustrated in Figure 4). Overall, the large volumes of melt water and freshly ground rock flour in subglacial environments suggests a role exists here for sorption and hydroxide precipitation processes.

Mineral saturation states were calculated using the PHREEQC program, (Parkhurst and Appelo, 1999) using measured concentration data from the DL, as well as in-situ pH, alkalinity and temperature data (see Supplementary Information for full details). The PHREEQC calculations indicate that all carbonate phases were under-saturated in the melt water, therefore while the precipitation of this phase may be discounted, fractionation due to the dissolution of carbonate phases remains possible. The supersaturated phases (Saturation Index (SI) > 1) in the meltwater are gibbsite, goethite and hematite. Iron (oxy)hydroxides progress from under-saturated to supersaturated at CD 235. The SI for these phases implies the presence of colloids in the meltwater. Therefore, minor and trace elements may be removed from solution as these phases precipitate, potentially causing stable isotope fractionation. If minerals containing alkaline earth elements are under-saturated and mobile in the DL they may interact with the SS surfaces. Oxy-hydroxides are highly sorbent materials and soluble (oxy)hydroxide-metal complexes are preferentially adsorbed onto Fe, Al and Mn oxy-hydroxide solids (Langmuir, 1997). Mitchell et al. (2001) suggested that many minor and trace elements present as hydroxide complexes, but not saturated in solution, may be adsorbed onto (oxy)hydroxide precipitates in subglacial and proglacial environments. X-Ray diffraction measurements of the SS also confirm the presence of clays e.g. vermiculite, montmorillonite (Section 4.3.3 and Supplementary Information) in the mineral assemblage. The alkaline conditions of the meltwater in this study favor adsorption of trace and minor elements onto these phases (Langmuir, 1997). The magnitude of the offsets in stable Sr isotopes between the DL and SS could be attributed to interactions with Fe, Al and Mn (oxy)hydroxide solids.

If we assume the initial (*i*) composition of the DL $\delta^{88/86}Sr_{DL}{}^{i}$ is the same as the rock value (average tonolite, crystalline carbonate and granodiorite), then over the course of secondary weathering processes, the DL evolves from $\delta^{88/86}Sr_{DL}{}^{i}$ = 0.24 ± 0.05 ‰ (2 s.d.) to $\delta^{88/86}Sr_{DL}{}^{t}$ to 0.31 ± 0.05 ‰ (2 s.d, average DL) via dissolution followed by the removal of the lighter isotope to secondary phases (average composition SS) $\delta^{88/86}Sr_{SS}$ = 0.18 ± 0.07 ‰ (2 s.d.) after time, *t*. The average DL is enriched by 0.07 ± 0.07 ‰ (2 s.d. propagated), and the SS is depleted compared to the DL by 0.13 ‰, which is 0.06 ± 0.09 ‰ (2 s.d. propagated) than $\delta^{88/86}Sr_{DL}{}^{i}$. Assuming our postulated $\delta^{88/86}Sr_{DL}{}^{i}$ value is correct, then the isotope budget between the DL and SS balances. However it is possible that the SS we sample is not representative of the bulk rock sitting on the subglacial streambed, rather the composition is skewed to reflect minerals that are physically and chemically more readily weathered. Factors such as the water-rock ratio, particle size, crushing, repeated wetting, and the availability of protons for weathering all contribute to the rate of solute acquisition in the DL from the SS (Brown et al., 1996), and thus their chemical and isotopic composition. Although it is difficult to evaluate the effect of dissolution of primary minerals in controlling Sr isotopic compositions, as the composition of these phases is not well constrained, our data strongly suggest indicate that secondary mineral formation plays a significant role.

Given the large variation in $^{87}Sr/^{86}Sr$ of local bedrock values, and the surrounding region (Kistler et al., 1993) there may also be an even greater variation in the $\delta^{88/86}Sr$ of host rocks not measured as part of this study, for example the $\delta^{88/86}Sr$ of the quartzite. Given that the quartzite in particular had a much more radiogenic value than the other measured rocks, and therefore its $\delta^{88/86}Sr$ isotope composition may have been equally as different, which could impart a distinctive composition to the dissolved load. However quartzites tend to be difficult to weather compared to other more reactive phases such as carbonates and commonly have low Sr contents compared to carbonates and feldspar-bearing rocks such as tonolites. Chao et al. (2015) suggested that a heavier dissolved load may also derive from either heavier Sr isotopes being more mobile under chemical weathering conditions, or minerals that contain higher $\delta^{88/86}Sr$ compositions are weathered more easily. Here Chao et al. (2015) favour the latter hypotheses (based on increasing $^{87}Sr/^{86}Sr$ ratios with the Rb/Sr ratio during mineral leaching with decreasing $\delta^{88/86}Sr$ values) and suggest that minerals with a high $^{87}Sr/^{86}Sr$ and Rb/Sr may have a low $\delta^{88/86}Sr$, and that this trend may be the result of isotopic fractionation of stable Sr during fractional crystallization. If this is the case then there may be a large variation in the $\delta^{88/86}Sr$ composition of bedrocks in the Lemon Creek watershed and that our measured rock samples are not a true representation of the region.

The seasonal variation in the magnitude of $\delta^{88/86}Sr$ between the DL and SS (between 0.07 to 0.2 ‰) could be attributed to a number of processes. Firstly, a reflection of the degree of secondary mineral production post primary mineral dissolution. In this scenario, larger fractionations between the DL and SS would be associated with extent of secondary mineral production, with the lighter isotopes of Sr being adsorbed or incorporated into clay, (oxy)hydroxide and/or other secondary phases. Smaller fractionations between the DL and SS would indicate a predominance of primary mineral dissolution. Secondly, changes in either the sediment and/or water residence times within the glacier. In this latter scenario, $\delta^{88/86}Sr_{DL}$ and $\delta^{88/86}Sr_{SS}$ may vary due to the exposure of fresh bedrock, potentially of a different mineralogy (and $\delta^{88/86}Sr$ composition). As the season progresses as subglacial hydrological networks move up glacier, resulting in the activation

and release sediments (or water) from different sources within the glacier, e.g. the Yukon-Tanan terrain, akin to the radiogenic Sr system.

These data, whilst novel, indicate that further information is required to investigate the fractionation of stable strontium isotopes accompanying primary and secondary weathering processes to discern mechanisms underlying the magnitude and direction of fractionation between individual phases. Leaching experiments may establish equilibrium fractionation conditions between freshly ground bedrock, SS and the DL, if incongruent weathering processes affect the stable Sr fractionation. In addition, a better characterization of the $\delta^{88/86}$Sr compositions bedrock types and minerals would establish either a dominance of hetero- or homogeneity amongst primary phases.

Changes in the fluxes of continental weathering to the oceans over glacial-interglacial cycles in the Quaternary have been suggested to result in imbalances in the oceanic Sr budgets, forcing strontium out of steady state with regards to input and outputs in the oceans (Armstrong, 1971; Capo and Depaolo, 1990; Mokadem et al., 2015; Vance et al., 2009). During deglaciation the retreat of continental ice sheets would have left behind significant amounts of fresh finely grained minerals highly susceptible to chemical weathering potentially causing a pulse in rapid chemical weathering 'post glacial weathering peak' (Vance et al., 2009), although direct evidence for this in the marine $^{87}Sr/^{86}Sr$ record has not been resolved at the current level of analytical precision (Mokadem et al., 2015). Ascertaining strontium isotope data from modern-day receding glacial environments provides an analogue for investigating previous deglaciations. Krabbenhöft et al. (2010) estimated the stable strontium isotope composition into the oceans during the last glacial maximum assuming isotope equilibrium between oceanic inputs and outputs during the last glacial maximum. Here Krabbenhöft et al. (2010) invoke the weathering of shelf carbonates exposed at low sea levels and the weathering of post-glacially exposed abundant fine-grained material to ascertain an input value of 0.24 ± 0.02 ‰. We find that the DLs we measured here are heavier than the postulated glacial input, but the SS, bedrocks and our theoretical $\delta^{88/86}Sr_{DL}{}^{i}$ are within error. However the values measured here are only representative of the LCG and not of an integrated global glacial strontium isotope input into the oceans.

## 6. Conclusions

Here we present radiogenic and stable strontium isotope compositions of the DL and SS from the outflow of a small maritime influenced glacier in Alaska. Over a one-month period during peak to late melt, we observe a trend to more radiogenic strontium isotope compositions indicating an increased input from a radiogenic phase. While radiogenic phases such as biotite are likely to contribute, the Rb/Sr ratios indicate the contribution of some other source material; in particular trace and major element data indicate an increase in the weathering of potentially radiogenic carbonate minerals. Radiogenic carbonate phases may be present in the subglacial metamorphosed sedimentary Yukon-Tanana terrain; as the melt season progresses the subglacial network may evolve to expose more chemically reactive bedrock and impart a more radiogenic signature to the dissolved load. However, future hydrological studies would be needed to confirm

this hypothesis.

X-Ray Diffraction measurements suggest that the lithology of the SS remains fairly constant throughout the sample period, representing input from both the Tonalite sills and Yukon-Tanana terrains. The consistency in mineralogy and minor variance in glacial discharge suggest that the trend toward more radiogenic composition is also likely due to changes in the proportion of primary weathering from exposure of different bedrock types over the melt season.

The stable strontium isotope values of both the SS and DL show little seasonal variability with an average of 0.18 ± 0.03 ‰ and 0.31 ± 0.05 ‰ respectively, and with an offset of approximately 0.1 to 0.2 ‰ between dissolved and solid phases. Local bedrocks lie between DL and SS values and range from ~0.20 to 0.26 ‰. We propose that the difference in stable strontium isotopic composition is driven by the extent of secondary mineral formation, resulting in preferential incorporation of the lighter isotopes, driving the dissolved load to heavier values. However, we cannot rule out incongruent fractionation of stable Sr isotopes from the dissolution of primary phases. The chemical weathering of subglacial sediment, followed by the formation of secondary weathering products, drives DL to heavier values as the lighter isotopes are incorporated into secondary weathering products akin to the $\delta^7$Li isotope. The magnitude of the offset between the SS and DL may vary due to both sorption and co-precipitation reactions, and released by de-sorption and dissolution processes.

The combination of stable and radiogenic strontium isotopes applied to weathering processes shows that radiogenic Sr isotopes provide information regarding incongruent weathering of primary phases. By contrast, stable Sr isotope variations most likely reflect the formation of secondary weathering minerals, which incorporate the light isotopes, driving the DL to heavier values and the SSs to lighter. Further information is required to understand the fractionation of stable strontium isotopes that accompanies both primary and secondary weathering processes to discern the mechanisms behind the magnitude and direction of fractionation between the phases.

**Acknowledgements**

Funding was provided by the Department of Earth & Environmental Sciences Turner Fellowship, University of Michigan to EIS and by the Packard Foundation to SMA. Thank you to Ted Huston for trace element analysis, University of Michigan Undergraduate Research Opportunity Program (UROP) students Nickolas Adamowicz, Rohan Mehta, Megan Wiltse and Anna Clinger for laboratory assistance and Kyle Meyer, Yi-Wei Liu, and Walt Afonso for field assistance, and to Philip Pogge von Strandmann and Phil Renforth for help with PHREEQC. We thank Christopher Pearce who provided help in to the interpretation, and the development of thinking through wider scale processes. We are very thankful to Tom Bullen for constructive input and insight to the first iterations of this manuscript. Additionally, the helpful and constructive reviews from Clement Bataille and the anonymous reviewer that greatly helped shape and focus the discussion and conclusions, as well as the editorial assistance from Michael E. Böttcher.

## 9. References


Aciego, S., Stevenson, E.I., Arendt, C.A., 2015. Climate versus geological controls on glacial meltwater micronutrient production in southern Greenland. Earth and Planetary Science Letters, 424: 51-58.

Aciego, S.M., Bourdon, B., Lupker, M., Rickli, J., 2009. A new procedure for separating and measuring radiogenic isotopes (U, Th, Pa, Ra, Sr, Nd, Hf) in ice cores. Chemical Geology, 266(3-4): 194-204.

Albarède, F., Beard, B., 2004. Analytical Methods for Non-Traditional Isotopes. In: Rosso, J.J. (Ed.), Reviews in Mineralogy and Geochemistry. Mineralogical Society of America. , pp. 113-152.

Anderson, S.P., Drever, J.I., Frost, C.D., Holden, P., 2000. Chemical weathering in the foreland of a retreating glacier. Geochimica Et Cosmochimica Acta, 64(7): 1173-1189.

Anderson, S.P., Drever, J.I., Humphrey, N.F., 1997. Chemical weathering in glacial environments. Geology, 25(5): 399-402.

Armstrong, R.l., 1971. Glacial Erosion and Variable Isotopic Composition of Strontium in Sea Water. Nature-Physical Science, 230(14): 132-133.

Arn, K., Hosein, R., Föllmi, K.B., 2003. Strontium isotope systematics in two glaciated crystalline catchments: Rhone and Oberaar Glaciers (Swiss Alps). Schweizerische mineralogische und petrographische Mitteilungen, 83: 273-283.

Benn, D.I., Evans, D.J.A., 2010. Glaciers and glaciation. Hodder Education, London.

Blum, J.D., Erel, Y., 1995. A Silicate Weathering Mechanism Linking Increases in Marine Sr-87/Sr-86 with Global Glaciation. Nature, 373(6513): 415-418.

Bohm, F., Eisenhauer, A., Tang, J. W., Dietzel, M., Krabbenhoft, A., Kisakurek, B., Horn, C., 2012. Strontium isotope fractionation of planktic foraminifera and inorganic calcite. Geochimica Et Cosmochimica Acta, 93: 300-314.

Böhm, F., Gussone, N., Eisenhauer, A., Dullo, W. C., Reynaud, S., Paytan, A., 2006. Calcium isotope fractionation in modern scleractinian corals. Geochimica Et Cosmochimica Acta, 70(17): 4452-4462.

Brennan, S.R. Fernandez, D. P., Mackey, G., Cerling, T. E., Bataille, C. P., Bowen, G. J., Wooller, M. J., 2014. Strontium isotope variation and carbonate versus silicate weathering in rivers from across Alaska: Implications for provenance studies. Chemical Geology, 389: 167-181.

Brew, D.A., Ford, A.B., 1985. Preliminary reconnaissance geologic map of the Juneau, Taku River, Atlin and part of the Skagway 1:250,000 quadrangles, southeastern Alaska, 2331-1258. US Geological Survey.

Brown, G.H., Sharp, M.J., Tranter, M., Gurnell, A.M., Nienow, P.W., 1994a. Impact of Post-Mixing Chemical-Reactions on the Major Ion Chemistry of Bulk Meltwaters Draining the Haut Glacier Darolla, Valais, Switzerland. Hydrological Processes, 8(5): 465-480.

Brown, G.H., Tranter, M., Sharp, M.J., 1996. Experimental investigations of the weathering of suspended sediment by Alpine glacial meltwater. Hydrological Processes, 10(4): 579-597.

Brown, G.H., Tranter, M., Sharp, M.J., Davies, T.D., Tsiouris, S., 1994b. Dissolved-Oxygen Variations in Alpine Glacial Meltwaters. Earth Surface Processes and Landforms, 19(3): 247-253.

Capo, R.C., Depaolo, D.J., 1990. Seawater Strontium Isotopic Variations from 2.5 Million Years Ago to the Present. Science, 249(4964): 51-55.

Chao, H.-C., You, C.-F., Liu, H.-C., Chung, C.-H., 2015. Evidence for stable Sr isotope fractionation by silicate weathering in a small sedimentary watershed in southwest Taiwan. Geochemica et Cosmochimica Acta, 165: 324-341.

Charlier, B.L.A., Ginibre, C., Morgan, D., Nowell, G. M., Pearson, D. G., Davidson, J. P., Ottley, C. J., 2006. Methods for the microsampling and high-precision analysis of strontium and rubidium isotopes at single crystal scale for petrological and geochronological applications. Chemical Geology, 232(3-4): 114-133.

Charlier, B.L.A., Nowell, G. M., Parkinson, I. J., Kelley, S. P., Pearson, D. G., Burton, K. W., 2012. High temperature strontium stable isotope behaviour in the early solar system and planetary bodies. Earth and Planetary Science Letters, 329: 31-40.

Criscitiello, A.S., Kelly, M.A., Tremblay, B., 2010. the responce of taku and Lemon Creek Glaciers to Climate. Arctic, Antarctic and Ampine Research, 42(1): 34-44.

Dasch, E.J., 1969. Strontium Isotopes in Weathering Profiles, Deep-Sea Sediments, and Sedimentary Rocks. Geochimica Et Cosmochimica Acta, 33(12): 1521-&.

de Souza, G.F., Reynolds, B.C., Kiczka, M., Bourdon, B., 2010. Evidence for mass-dependent isotopic fractionation of strontium in a glaciated granitic watershed. Geochimica Et Cosmochimica Acta, 74(9): 2596-2614.

Douglas, T.A., Blum, J.D., Guo, L., Keller, K., Gleason, J.D., 2013. Hydrogeochemistry of seasonal flow regimes in the Chena River, a subarctic watershed draining discontinuous permafrost in interior Alaska (USA). Chemical Geology, 335: 48-62.

767 Fairchild, I.J., Bradby, L., Sharp, M., Tison, J.L., 1994. Hydrochemistry of Carbonate Terrains in
768 Alpine Glacial Settings. Earth Surface Processes and Landforms, 19(1): 33-54.

769 Fairchild, I.J., Killawee, J.A., Hubbard, B., Dreybrodt, W., 1999. Interactions of calcareous
770 suspended sediment with glacial meltwater: a field test of dissolution behaviour.
771 Chemical Geology, 155(3-4): 243-263.

772 Fietzke, J., Eisenhauer, A., 2006. Determination of temperature-dependent stable strontium
773 isotope (Sr-88/Sr-86) fractionation via bracketing standard MC-ICP-MS. Geochemistry
774 Geophysics Geosystems, 7.

775 Fountain, A.G., Walder, J.S., 1998. Water flow through temperate glaciers. Reviews of
776 Geophysics, 36(3): 299-328.

777 Gehrels, G.E., Brew, D.A., Saleeby, J., 1984. Progress report on U/Pb (zircon) geochronologic
778 studies in the Coast plutonic-metamorphic complex east of Juneau, southeastern Alaska.
779 The United States Geological Survey in Alaska; accomplishments during 1982: U.S.
780 Geological Survey Circular 939.

781 Hagedorn, B., Hasholt, B., 2004. Hydrology, geochemistry and Sr isotopes in solids and solutes
782 of the meltwater from Mittivakkat Gletscher, SE Greenland. Nordic Hydrology, 35(4-5):
783 369-380.

784 Halicz, L., Segal, I., Fruchter, N., Stein, M., Lazar, B., 2008. Strontium stable isotopes fractionate
785 in the soil environments? Earth and Planetary Science Letters, 272(1-2): 406-411.

786 Heusser, C.J., Marcus, M.G., 1960. Glaciological and related studies of Lemon Creek Glacier,
787 Alaska. Final report: Juneau Icefield Research Project, New York.

788 Hindshaw, R.S., Reynolds, B.C., Bourdon, B., Wiederhold, J.G., Kretzschmar, R., 2008. Calcium
789 isotope variations at the Damma glacier, Switzerland. Geochimica Et Cosmochimica
790 Acta, 72(12): A378-A378.

791 Hindshaw, R.S., Reynolds, B.C., Wiederhold, J.G., Kretzschmar, R., Bourdon, B., 2011. Calcium
792 isotopes in a proglacial weathering environment: Damma glacier, Switzerland.
793 Geochimica Et Cosmochimica Acta, 75(1): 106-118.

794 Hodson, A.J., Ferguson, R.I., 1999. Fluvial suspended sediment transport from cold and warm-
795 based glaciers in Svalbard. Earth Surface Processes and Landforms, 24(11): 957-974.

796 Hooke, R.L., 1989. Englacial and Subglacial Hydrology - a Qualitative Review. Arctic and
797 Alpine Research, 21(3): 221-233.

798 Ingram, G.M., Hutton, D.H.W., 1994. The Great Tonalite Sill - Emplacement into a Contractional
799 Shear Zone and Implications for Late Cretaceous to Early Eocene Tectonics in

800 Southeastern Alaska and British-Columbia. Geological Society of America Bulletin,
801 106(5): 715-728.

802 Kistler, R.W., Newberry, R.J., Brew, D.A., 1993. Rubidium-strontium isotopic systematics of
803 vein minerals in the Juneau gold belt, Alaska. In: Dusel-Bacon, C., Till, A.B. (Eds.),
804 Geologic studies in Alaska by the U.S. Geological Survey: U.S. Geological Survey
805 Bulletin 2068, pp. 236-240.

806 Krabbenhöft, A. et al., 2010. Constraining the marine strontium budget with natural strontium
807 isotope fractionations ((87)Sr/(86)Sr*, delta(88/86)Sr) of carbonates, hydrothermal
808 solutions and river waters. Geochimica Et Cosmochimica Acta, 74(14): 4097-4109.

809 Krabbenhöft, A. et al., 2009. Determination of radiogenic and stable strontium isotope ratios
810 ((87)Sr/(86)Sr; delta(88/86)Sr) by thermal ionization mass spectrometry applying an
811 (87)Sr/(84)Sr double spike. Journal of Analytical Atomic Spectrometry, 24(9): 1267-
812 1271.

813 Langmuir, D., 1997. The use of laboratory adsorption data and models to predict radionuclide
814 releases from a geological repository: A brief history. Scientific Basis for Nuclear Waste
815 Management Xx, 465: 769-780.

816 Liu, H.-C., You, C.-F., Tu, Y.J., 2012. Stable strontium isotopic fractionation during adsorption
817 onto magnetic nano-humic acid coated iron oxide particles, EGU General Assembly,
818 Vienna, Austria.

819 Ma, J.L., Wei, G. J., Liu, Y., Ren, Z. Y., Xu, Y. G., Yang, Y. H., 2013. Precise measurement of
820 stable (delta Sr-88/86) and radiogenic (Sr-87/Sr-86) strontium isotope ratios in geological
821 standard reference materials using MC-ICP-MS. Chinese Science Bulletin, 58(25): 3111-
822 3118.

823 Miller, M.M., Pelto, M.S., 1999. Mass Balance Measurements on the Lemon Creek Glacier,
824 Juneau icefield Alaska 1953-1998. Geografiska Annaler 81 A(4): 617-681.

825 Millot, R., Gaillardet, J., Dupré, B., Allegre, C.J., 2003. Northern latitude chemical weathering
826 rates: Clues from the Mackenzie River Basin, Canada. Geochemica et Cosmochimica
827 Acta, 67(7): 1305-1329.

828 Millot, R., Vigier, N., Gaillardet, J., 2010. Behaviour of lithium and its isotopes during
829 weathering in the Mackenzie Basin, Canada. Geochimica Et Cosmochimica Acta, 74(14):
830 3897-3912.

831 Mitchell, A., Brown, G.H., Fuge, R., 2001. Minor and trace element export from a glacierized
832 Alpine headwater catchment (Haut Glacier d'Arolla, Switzerland). Hydrological
833 Processes, 15(18): 3499-3524.

Mokadem, F., Parkinson, I. J., Hathorne, E. C., Anand, P., Allen, J. T., Burton, K. W., 2015. High-precision radiogenic strontium isotope measurements of the modern and glacial ocean: Limits on glacial-interglacial variations in continental weathering. Earth and Planetary Science Letters, 415: 111-120.

Moynier, F., Agranier, A., Hezel, D.C., Bouvier, A., 2010. Sr stable isotope composition of Earth, the Moon, Mars, Vesta and meteorites. Earth and Planetary Science Letters, 300(3-4): 359-366.

Nienow, P.W., Sharp, M., Willis, I.C., 1996. Velocity-discharge relationships derived from dye tracer experiments in glacial meltwaters: Implications for subglacial flow conditions. Hydrological Processes, 10(10): 1411-1426.

NOAA, 2014. Quality Controlled Local Climatological Data (QCLCD 2.5.5). NOAA-ESRL Physical Sciences Division, Boulder Colorado

Ohno, T., Komiya, T., Ueno, Y., Hirata, T., Maruyama, S., 2008. Determination of Sr-88/Sr-86 mass-dependent isotopic and radiogenic isotope variation of Sr-87/Sr-86 in the Neoproterozoic Doushantuo Formation. Gondwana Research, 14(1-2): 126-133.

Parkhurst, D.L., Appelo, C.A.J., 1999. User's guide to PHREEQC (version 2)--A computer program for speciation, batch-reaction, one-dimensional transport, and inverse geochemical calculations. U.S. Geological Survey Water-Resources Investigations Report 99-4259, 99-4259: 312.

Pearce, C.R., Parkinson, I. J., Gaillardet, J., Charlier, B. L. A., Mokadem, F., Burton, K. W.,, 2015. Reassessing the stable (δ88/86Sr) and radiogenic (87Sr/86Sr) strontium isotope composition of marine inputs. Geochemica et Cosmochimica Acta, 157: 125-146.

Pogge von Strandmann, P.A.E., Burton, K. W., James, R. H., van Calsteren, P., Gislason, S. R., Mokadem, F., 2006. Riverine behaviour of uranium and lithium isotopes in an actively glaciated basaltic terrain. Earth and Planetary Science Letters, 251(1-2): 134-147.

Rüggeberg, A., Fietzke, J., Liebetrau, V., Eisenhauer, A., Dullo, W. C., Freiwald, A., 2008. Stable strontium isotopes (delta Sr-88/86) in cold-water corals - A new proxy for reconstruction of intermediate ocean water temperatures. Earth and Planetary Science Letters, 269(3-4): 569-574.

Sharp, M., Creaser, R.A., Skidmore, M., 2002. Strontium isotope composition of runoff from a glaciated carbonate terrain. Geochimica Et Cosmochimica Acta, 66(4): 595-614.

Sheik, C.S., Stevenson, E. I., Den Uyl, P. A., Arendt, C. A., Aciego, S. M., Dick, G. J., 2015. Microbial communities of the Lemon Creek Glacier show subtle structural variation yet stable phylogenetic composition over space and time. Frontiers in Microbiology, 6.

868 Stevenson, E.I., Hermoso, M., Rickaby, R. E. M., Tyler, J. J., Minoletti, F., Parkinson, I. J.,
869 Mokadem, F., Burton, K. W., 2014. Controls on stable strontium isotope fractionation in
870 coccolithophores with implications for the marine Sr cycle. Geochimica Et
871 Cosmochimica Acta, 128: 225-235.

872 Swift, D.A., Nienow, P.W., Hoey, T.B., 2005. Basal sediment evacuation by subglacial
873 meltwater: suspended sediment transport from Haut Glacier d'Arolla, Switzerland. Earth
874 Surface Processes and Landforms, 30(7): 867-883.

875 Tipper, E.T., Lemarchand, E., Hindshaw, R.S., Reynolds, B.C., Bourdon, B., 2012. Seasonal
876 sensitivity of weathering processes: Hints from magnesium isotopes in a glacial stream.
877 Chemical Geology, 312: 80-92.

878 Tranter, M., 2003. Geochemical weathering in glacial and proglacial environments. In: Drever,
879 J.I. (Ed.), Surface and Ground Water, Weathering, and Soils, Vol. 5 Elsevier, pp. 189 -
880 205.

881 Tranter, M., Brown, G., Raiswell, R., Sharp, M., Gurnell, A., 1993. A Conceptual-Model of
882 Solute Acquisition by Alpine Glacial Meltwaters. Journal of Glaciology, 39(133): 573-
883 581.

884 Vance, D., Teagle, D.A.H., Foster, G.L., 2009. Variable Quaternary chemical weathering fluxes
885 and imbalances in marine geochemical budgets. Nature, 458(7237): 493-496.

886 Vigier, N., Decarreau, A., Millot, R., Carignan, J., Petit, S., France-Lanord, C.., 2008.
887 Quantifying Li isotope fractionation during smectite formation and implications for the
888 Li cycle. Geochimica Et Cosmochimica Acta, 72(3): 780-792.

889 Voss, B.M., Peucker-Ehrenbrink, B., Eglinton, T.I., Fiske, G., Wang, Z.A., Hoering, K.A.,
890 Montluçon, D.B., LeCroy, C., Pal, S., Marsh, S., Gillies, S.L., Janmaat, A., Bennett, M. ,
891 Downey, B., Fanslau, J., Fraser, H., Macklam-Harron, G., Martinec, M., Wiebe, B..,
892 2014. Tracing river chemistry in space and time: Dissolved inorganic constituents of the
893 Fraser River, Canada. Geochemica et Cosmochimica Acta, 124: 283-308.

894 Wei, G.J., Ma, J. L., Liu, Y., Xie, L. H., Lu, W. J., Deng, W. F., Ren, Z. Y., Zeng, T., Yang, Y.
895 H., 2013. Seasonal changes in the radiogenic and stable strontium isotopic composition
896 of Xijiang River water: Implications for chemical weathering. Chemical Geology, 343:
897 67-75.

898 White, A.F., Schulz, M.S., Lowenstern, J.B., Vivit, D.V., Bullen, T.D., 2005. The ubiquitous
899 nature of accessory calcite in granitoid rocks: Implications for weathering, solute
900 evolution, and petrogenesis. Geochimica Et Cosmochimica Acta, 69(6): 1455-1471.

901 Widanagamage, I.H., Schauble, E.A., Scher, H.D., M., E., Griffith, E.M., 2014. Stable strontium
902 isotope fractionation in synthetic barite. Geochimica et Cosmochimica Acta, Accepted
903 Manuscript(doi: 10.1016/j.gca.2014.10.004).

Wimpenny, J., Burton, K. W., James, R. H., Gannoun, A., Mokadem, F., Gislason, S. R., 2011. The behaviour of magnesium and its isotopes during glacial weathering in an ancient shield terrain in West Greenland. Earth and Planetary Science Letters, 304(1-2): 260-269.

Wimpenny, J., James, R. H., Burton, K. W., Gannoun, A., Mokadem, F., Gislason, S. R., 2010. Glacial effects on weathering processes: New insights from the elemental and lithium isotopic composition of West Greenland rivers. Earth and Planetary Science Letters, 290(3-4): 427-437.

Wombacher, F., Eisenhauer, A., Bohm, F., Gussone, N., Regenberg, M., Dullo, W. C., Ruggeberg, A., 2011. Magnesium stable isotope fractionation in marine biogenic calcite and aragonite. Geochimica Et Cosmochimica Acta, 75(19): 5797-5818.

**Figure captions:**

Figure 1: Location maps. (a) Location of the field site in coastal southeastern Alaska. (b) Main panel: Lemon Creek glacier size and topography with the local extent of Thomas Glacier in the top right. Local geology: KPs = Taku Terrain, part of the Juneau Goldbelt composed of Greenschist facies metamorphosed sedimentary rocks, late Permian. TKt = tonalite sills, 50-70 Ma. pTMsv = Yukon-Tanana Terrane, high grade metamorphosed sedimentary and volcanic rocks, Cretaceous to Proterozoic in age (Brewer and Ford, 1985; Kistler et al., 1993; Samson et al., 1990). Insert: Watershed limits of the Lemon Creek Glacier. The outlines of the glaciers are shown in grey (Lemon Creek Glacier, right, and the local extent of Thomas Glacier top right). The red region shows the limits of the Lemon Creek Glacier watershed, see Section 2. (c) Satellite image of the sample site highlighting the inputs into Lake Thomas from the Thomas and Lemon Creek Glaciers. A: Glacial terminus where daily sampling took place, B: Location of daily discharge measurements (See section 3.1). Blue lines indicate where the streams flow between the glaciers (Thomas Glacier and lemon Creek Glacier) and the lakes (Lake Thomas and the Lower Lake).

Figure 2: Daily measurements from the Lemon Creek Glacier: Upper two panels, hydrochemistry; (a) Strontium concentrations (left axis) as measured in the filtered dissolved load compared to in stream conductivity measurements (right axis). (b) Daily measurements of discharge measured from the LCG outflow into Lake Thomas (left axis) as measured at location 'B' on figure 1 (c), compared to the weighted sediment load per litre taken from the glacial terminus (right axis). Lower two panels, strontium isotope compositions; (c) radiogenic and (d) stable compositions of the dissolved load (open symbols) and suspended sediment (black symbols) from the Lemon Creek Glacier melt water between from the $10^{th}$ August to the $8^{th}$ Sept 2012 (Calendar day (CD) 223 – 252). The blue line is the average weighted global river average (with two standard deviation in blue error envelope) from Krabbenhöft et al. (2010). The brown line (with two standard deviation in brown error envelope) is the bulk silicate Earth average from Moynier et al. (2010).

Figure 3: Concentration and isotope compositions in the dissolved loads of the Lemon Creek glacier as a function of calendar day (CD). (a) Correlation of radiogenic Sr isotopes with Rb/Sr ratios as a function of time, $R^2$=0.62. (b) Evolution of $^{87}Sr/^{86}Sr$ and Ca/Mg as a function of time: As time increases we see an increase in the Ca/Mg and trends towards more radiogenic $^{87}Sr/^{86}Sr$ values. (c) Evolution of $\delta^{88/86}Sr$ and Ca/Mg as a function of time: As time increases we see an increase in both the Ca/Mg and $\delta^{88/86}Sr$, however this is not the expected direction of $\delta^{88/86}Sr$ fractionation if carbonate weathering is increasing with time suggesting changes in these parameters (and the $^{87}Sr/^{86}Sr$ and Ca/Mg plot) are decoupled.

Figure 4: Triple isotope plot of $^{87}Sr/^{86}Sr$ versus $\delta^{88/86}Sr$, illustrating the difference in composition between the bedrock, suspended sediment and dissolved load. Insert shows the direction we would expect the radiogenic and stable isotopes to progress given an increase in silicate or carbonate weathering into the glacial outflow assuming congruent weathering into the dissolved load. Here the radiogenic Sr ratio is showing primary mineral dissolution, and the stable Sr ratio the degree of secondary mineral formation, which drives the fractionation between the dissolved load (open symbols) and suspended sediment (filled symbols). [1] Shaded area is the bulk silicate earth average from Moynier et al. (2010). [2] Modern riverine input and estimated glacial (Last Glacial Maximum) input values are from Krabbenhöft et al. (2010).

Table 1: Daily major and trace element concentrations as well as both radiogenic and stable isotopic data of the dissolved load and suspended sediments in the bulk outflow form Lemon Creek glacier over the 10$^{th}$ August to the 8$^{th}$ Sept 2012 (Calendar day (CD) 223 to 252).

Supplemental Information A: Sampling methods and raw data for daily *in situ* measurements from the Lemon Creek Glacier, with air temperature and precipitation data taken the local weather station at Juneau airport (data is from NOAA) and matched field meterological observations. Mineral saturation state calculation output using PHREEQC (Pankhurst and Appello, 1990). Mineral saturation states are reported in Saturation Index (SI) units for daily measurements, where available. Comparison of Lemon Creek XRD profiles of suspended sediment on CD 223, 235 and 249 2012. Comparison of Lemon Creek XRD profiles of suspended sediment between the beginning and end of the season.

Figure 1

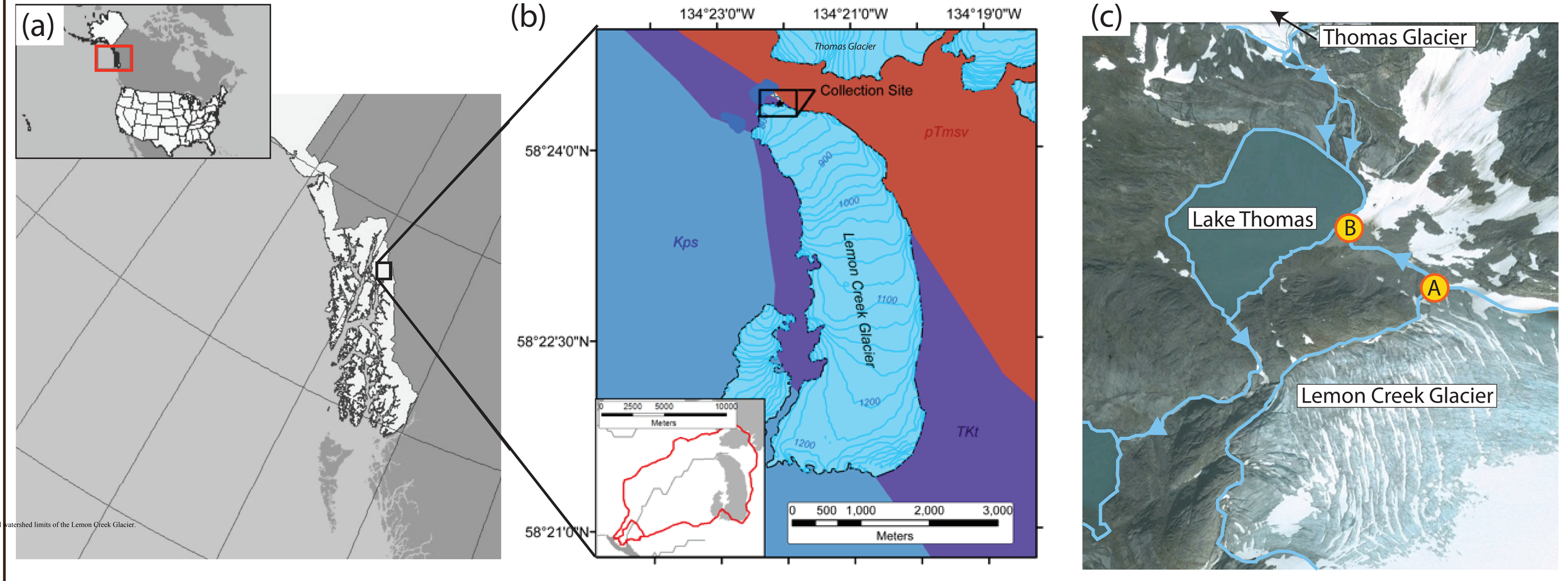


and watershed limits of the Lemon Creek Glacier.

Figure 2

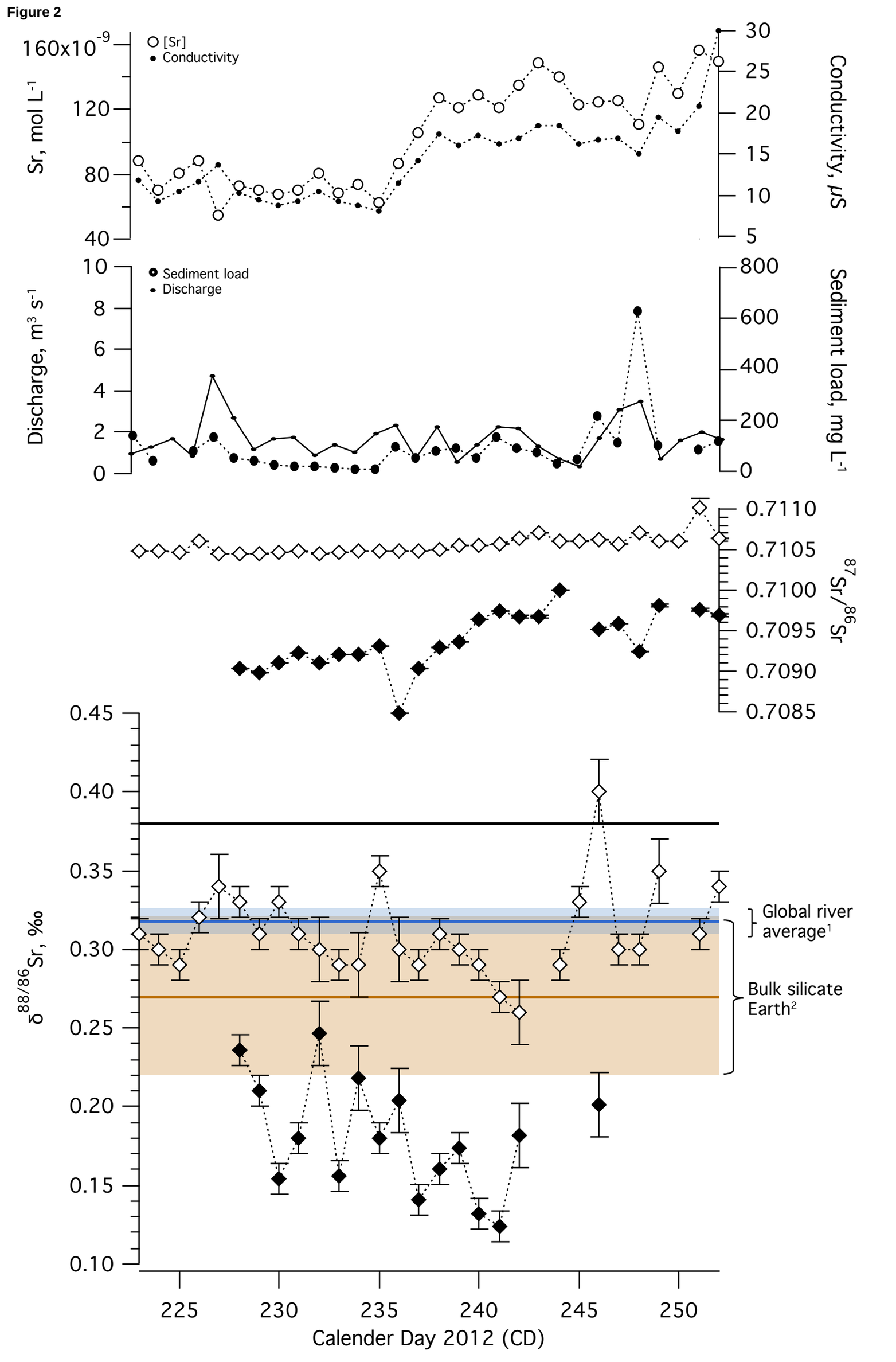
[Sr]
Conductivity
Sr, mol L-1
Conductivity, µS
Sediment load
Discharge
Discharge, m3 s-1
Sediment load, mg L-1
87Sr/86Sr
δ88/86Sr, ‰
Global river average1
Bulk silicate Earth2
Calender Day 2012 (CD)

Figure 3

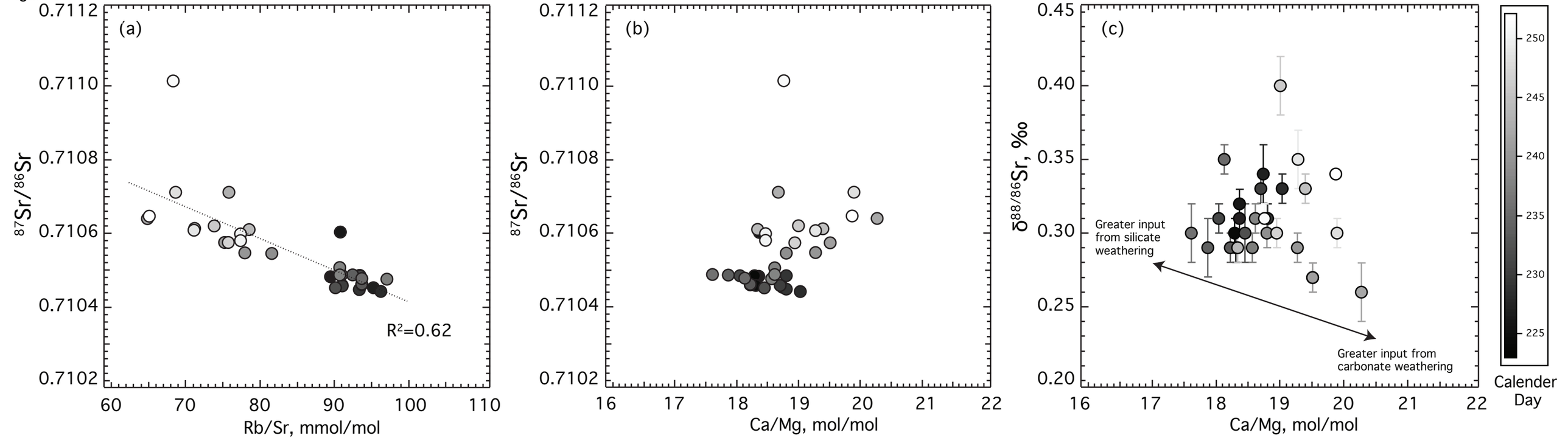
(a)
(b)
(c)
$^{87}Sr/^{86}Sr$
$\delta^{88/86}Sr$, ‰
Rb/Sr, mmol/mol
Ca/Mg, mol/mol
$R^2$=0.62
Greater input from silicate weathering
Greater input from carbonate weathering
Calender Day

Figure 4

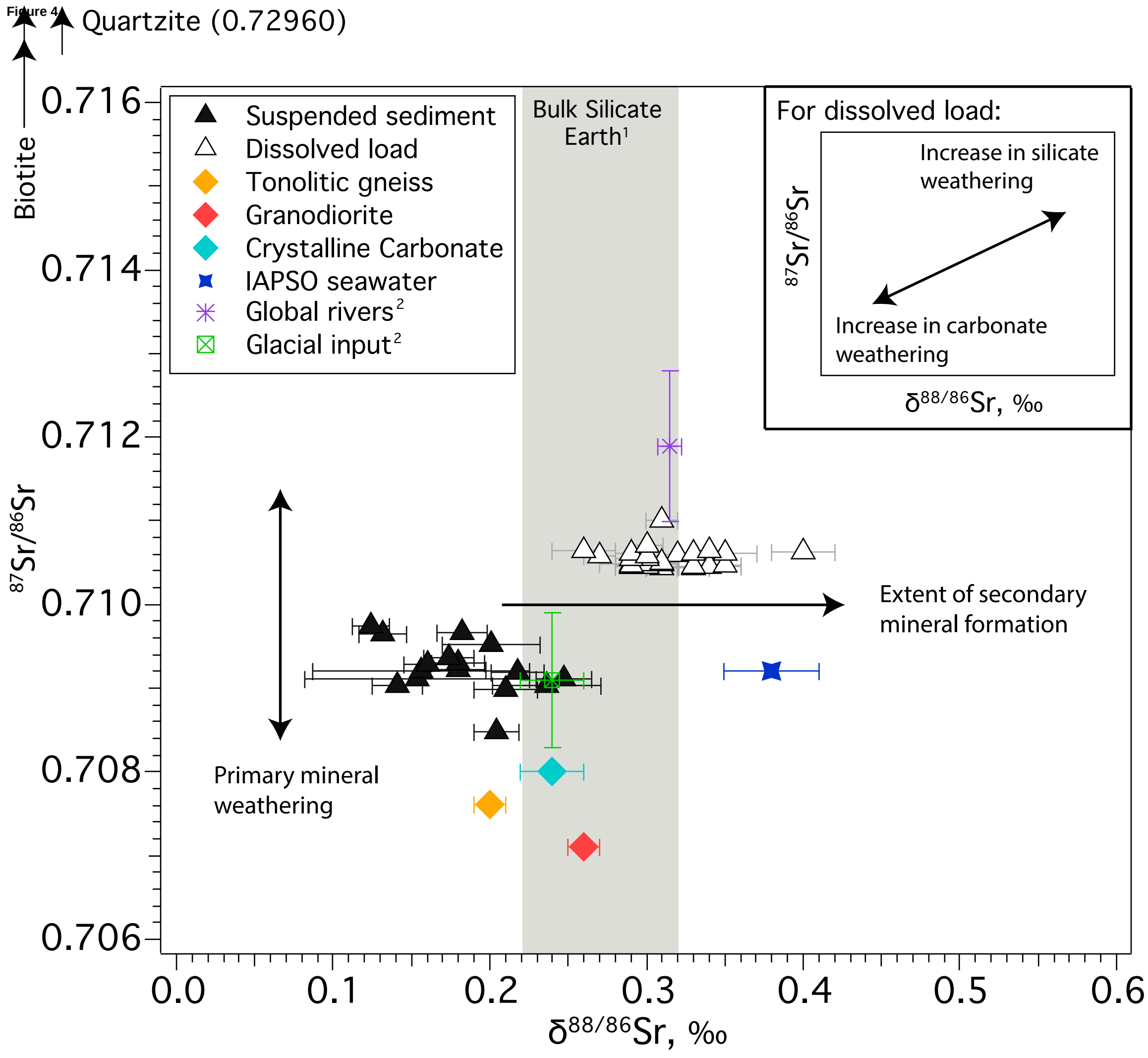
Quartzite (0.72960)
Biotite
0.716
0.714
0.712
0.710
0.708
0.706
$^{87}Sr/^{86}Sr$
Suspended sediment
Dissolved load
Tonolitic gneiss
Granodiorite
Crystalline Carbonate
IAPSO seawater
Global rivers[2]
Glacial input[2]
Bulk Silicate Earth[1]
For dissolved load:
Increase in silicate weathering
Increase in carbonate weathering
$^{87}Sr/^{86}Sr$
$\delta^{88/86}Sr$, ‰
Extent of secondary mineral formation
Primary mineral weathering
0.0
0.1
0.2
0.3
0.4
0.5
0.6
$\delta^{88/86}Sr$, ‰

**Table 1**

**Click here to download Table: CG 2015 EIS T1.xlsx**

Table 1

Table 1: Daily major and trace elemental concentrations with radiogenic and stable Sr measurements of the dissolved load of the Lemon creek glacier melt water between the 10th A
DL = dissolved load, SS = suspended sediment

| CD 2012 | Ca µmol/L | K µmol/L | Mg µmol/L | Na µmol/L | Sr µmol/L | Ba µmol/L | Rb µmol/L | $^{87}Sr/^{86}Sr$ (DL) | 2 s.e. | $^{87}Sr/^{86}Sr$ (SS) | 2 s.e. | $\delta^{88/86}Sr$ (DL) ‰ | 2 s.e. | $\delta^{88/86}Sr$ (SS) ‰ | 2 s.e. |
|---|---|---|---|---|---|---|---|---|---|---|---|---|---|---|---|
| 223 | 91.113 | 8.898 | 8.181 | 6.464 | 88.308 | 56.171 | 8.1 | 0.710483 | 0.000005 | - | - | 0.31 | 0.01 | - | - |
| 224 | 71.811 | 7.030 | 6.474 | 5.194 | 70.105 | 44.608 | 6.7 | 0.710485 | 0.000005 | - | - | 0.30 | 0.01 | - | - |
| 225 | 82.234 | 7.368 | 7.407 | 5.613 | 80.981 | 50.511 | 7.6 | 0.710459 | 0.000005 | - | - | 0.29 | 0.01 | - | - |
| 226 | 88.769 | 8.281 | 7.970 | 5.889 | 88.463 | 55.355 | 8.2 | 0.710603 | 0.000005 | - | - | 0.32 | 0.01 | - | - |
| 227 | 56.306 | 5.453 | 4.955 | 3.836 | 54.516 | 34.021 | 5.3 | 0.710453 | 0.000005 | - | - | 0.34 | 0.02 | - | - |
| 228 | 74.215 | 6.969 | 6.430 | 5.387 | 72.592 | 47.844 | 7.2 | 0.710442 | 0.000005 | 0.709036 | 0.000006 | 0.33 | 0.01 | 0.24 | 0.03 |
| 228 repeat | 0.000 | 0.000 | 0.000 | 0.000 | 0.000 | 0.000 | 0.0 | | | 0.709050 | 0.000006 | - | - | - | - |
| 229 | 69.688 | 7.004 | 6.112 | 4.860 | 70.321 | 46.217 | 6.7 | 0.710446 | 0.000008 | 0.708979 | 0.000006 | 0.31 | 0.01 | 0.21 | 0.02 |
| 229 repeat | 0.000 | 0.000 | 0.000 | 0.000 | 0.000 | 0.000 | 0.0 | 0.710448 | 0.000005 | 0.709093 | 0.000006 | 0.30 | 0.01 | - | - |
| 230 | 67.808 | 6.350 | 5.979 | 4.512 | 67.963 | 43.643 | 6.3 | 0.710458 | 0.000005 | 0.709109 | 0.000006 | 0.33 | 0.01 | 0.15 | 0.07 |
| 231 | 68.332 | 6.866 | 6.244 | 4.940 | 70.323 | 46.041 | 6.7 | 0.710484 | 0.000005 | 0.709223 | 0.000006 | 0.31 | 0.01 | 0.18 | 0.02 |
| 232 | 78.125 | 7.282 | 6.981 | 5.219 | 80.373 | 51.334 | 7.4 | 0.710452 | 0.000005 | 0.709110 | 0.000005 | 0.30 | 0.02 | 0.25 | 0.02 |
| 233 | 67.820 | 6.791 | 6.138 | 4.416 | 68.393 | 43.823 | 6.6 | 0.710460 | 0.000006 | 0.709214 | 0.000007 | 0.29 | 0.01 | 0.16 | 0.10 |
| 233 repeat | 0.000 | 0.000 | 0.000 | 0.000 | 0.000 | 0.000 | 0.0 | 0.710462 | 0.000006 | 0.709096 | 0.000007 | - | - | 0.18 | 0.02 |
| 234 | 69.126 | 7.112 | 6.380 | 4.706 | 73.362 | 47.092 | 7.0 | 0.710487 | 0.000006 | 0.709198 | 0.000006 | 0.29 | 0.02 | 0.22 | 0.02 |
| 235 | 60.722 | 5.919 | 5.523 | 4.131 | 62.795 | 41.122 | 6.0 | 0.710478 | 0.000005 | 0.709302 | 0.000006 | 0.35 | 0.01 | 0.18 | 0.02 |
| 235 repeat | 0.000 | 0.000 | 0.000 | 0.000 | 0.000 | 0.000 | 0.0 | | | 0.709331 | 0.000005 | | | 0.20 | 0.03 |
| 236 | 85.455 | 8.074 | 8.002 | 5.803 | 86.860 | 58.208 | 8.1 | 0.710488 | 0.000006 | 0.708487 | 0.000006 | 0.30 | 0.02 | 0.20 | 0.01 |
| 237 | 104.964 | 10.164 | 9.322 | 6.522 | 105.796 | 70.904 | 10.5 | 0.710476 | 0.000005 | 0.709040 | 0.000006 | 0.29 | 0.01 | 0.14 | 0.02 |
| 238 | 124.991 | 11.339 | 11.071 | 7.415 | 127.106 | 87.426 | 11.8 | 0.710507 | 0.000005 | 0.709287 | 0.000005 | 0.31 | 0.01 | 0.16 | 0.01 |
| 238 repeat | 0.000 | 0.000 | 0.000 | 0.000 | 0.000 | 0.000 | 0.0 | 0.710488 | 0.000006 | 0.709411 | 0.000006 | - | - | - | - |
| 239 | 116.990 | 10.845 | 10.262 | 6.853 | 121.666 | 82.686 | 10.2 | 0.710546 | 0.000005 | 0.709360 | 0.000007 | 0.30 | 0.01 | 0.17 | 0.02 |
| 240 | 125.522 | 11.832 | 10.738 | 6.873 | 128.748 | 89.329 | 10.3 | 0.710547 | 0.000006 | 0.709644 | 0.000005 | 0.29 | 0.01 | 0.13 | 0.02 |
| 241 | 116.029 | 11.672 | 9.806 | 6.773 | 121.211 | 77.333 | 9.3 | 0.710575 | 0.000006 | 0.709743 | 0.000006 | 0.27 | 0.01 | 0.12 | 0.01 |
| 241 repeat | 0.000 | 0.000 | 0.000 | 0.000 | 0.000 | 0.000 | 0.0 | | | 0.709410 | 0.000005 | 0.28 | 0.01 | - | - |
| 242 | 131.730 | 13.883 | 10.716 | 9.302 | 135.302 | 90.682 | 9.0 | 0.710641 | 0.000005 | 0.709672 | 0.000010 | 0.26 | 0.02 | 0.18 | 0.02 |
| 243 | 139.908 | 14.166 | 12.355 | 8.180 | 148.905 | 105.344 | 11.6 | 0.710711 | 0.000006 | 0.709672 | 0.000010 | - | - | - | - |
| 244 | 137.365 | 13.536 | 12.350 | 7.784 | 140.289 | 93.395 | 11.3 | 0.710610 | 0.000005 | 0.710003 | 0.000008 | 0.29 | 0.01 | - | - |
| 245 | 117.636 | 11.587 | 10.001 | 6.376 | 122.903 | 85.134 | 9.0 | 0.710613 | 0.000006 | - | - | 0.33 | 0.01 | - | - |
| 246 | 119.946 | 11.666 | 10.410 | 7.289 | 124.427 | 86.127 | 9.4 | 0.710621 | 0.000008 | 0.709525 | 0.000005 | 0.40 | 0.02 | 0.20 | 0.03 |
| 247 | 120.388 | 11.800 | 10.479 | 7.366 | 125.351 | 81.478 | 9.7 | 0.710575 | 0.000006 | 0.709589 | 0.000006 | 0.30 | 0.01 | - | - |
| 248 | 116.848 | 12.260 | 9.684 | 5.823 | 111.240 | 64.932 | 7.8 | 0.710712 | 0.000006 | 0.709236 | 0.000005 | 0.30 | 0.01 | - | - |
| 249 | 144.772 | 14.248 | 12.383 | 10.181 | 146.464 | 95.188 | 10.7 | 0.710608 | 0.000006 | 0.709819 | 0.000009 | 0.35 | 0.02 | - | - |
| 250 | 121.930 | 12.096 | 10.888 | 11.507 | 129.727 | 90.144 | 10.3 | 0.710599 | 0.000005 | - | - | - | - | - | - |
| 250 repeat | 0.000 | 0.000 | 0.000 | 0.000 | 0.000 | 0.000 | 0.0 | 0.710580 | 0.000007 | - | - | - | - | - | - |
| 251 | 150.928 | 15.701 | 13.267 | 11.100 | 157.008 | 110.346 | 11.0 | 0.711014 | 0.000005 | 0.709751 | 0.000012 | 0.31 | 0.01 | - | - |
| 252 | 141.630 | 13.522 | 11.752 | 8.961 | 149.434 | 91.993 | 10.0 | 0.710647 | 0.000005 | 0.709693 | 0.000018 | 0.34 | 0.01 | - | - |
| | | | | | | | | | | | | | | | |
| Quartzite | | | | | | | | | | 0.729674 | 0.000014 | | | - | - |
| Gneiss | | | | | | | | | | 0.707618 | 0.000004 | | | 0.20 | 0.01 |
| Granodiorite | | | | | | | | | | 0.707100 | 0.000004 | | | 0.26 | 0.01 |
| Crystalline Carbonate | | | | | | | | | | 0.708000 | 0.000021 | | | 0.24 | 0.02 |

**Background dataset for online publication only**

**Click here to download Background dataset for online publication only: CG 2015 EIS SI.docx**